Experimental study on monotonic to high-cyclic behaviour of sand-silt mixtures

Merita Tafili[1] · Lukas Knittel[2] · Vera Gauger[3] · Torsten Wichtmann[1] · Hans Henning Stutz[3]

Abstract

The naturally deposited soil usually does not consist of pure coarse or fine-grained soil but of a mixture of both. The mechanical behaviour of a saturated fine sand mixed with varying amounts of low-plastic fines was evaluated by monotonic as well as high-cyclic triaxial tests. The test results were used to conclude on the effect of fines content on the critical state, phase transformation line, secant Young's modulus, the residual strain accumulation as well as strain amplitude during drained cycles of the mixtures in relation to the global void ratio as well as to the equivalent void ratio. It was found that while the choice of void ratio definition is important for the uniqueness of the critical void ratio, both approaches can be used as state variables for the phase transformation line. However, some seemingly contradictive results are found from the drained high-cyclic tests. Eventhough, an increase of the residual strain accumulation with decreasing fines content compared at the same initial equivalent void ratio is rendered by the laboratory data, a unique and on fines content independent relationship between ε^{acc} could be established only with respect to the initial global void ratio.

1 Introduction

The naturally deposited soil usually does not consist of pure coarse or fine-grained soil but of a mixture of both. Silty sands are the most common type of soil involved in both static and earthquake-induced liquefaction [4, 5, 7, 20, 30, 31, 33]. These soils are found abundantly in natural strata such as colluvium deposits, rockfills, underground of offshore foundations, alluvial deposits and glacial tills among others [19]. Similarly, in many man-made constructions, including embankments, in the mining industry in e.g. tailings dams and roadbeds, different percentages of fines contents may be used.

The influence of non-plastic fines content on the mechanical behaviour of sands has been the subject of several works during the last decades. However, little information regarding the influence of low to medium-plasticity fines content on the cumulative strains under drained cyclic loading can be found in the literature [12]. Cyclic simple shearing of dry mixtures of various sands with certain amounts of low-plasticity fines [35] showed a reduction of the deformation after 15 cycles with increasing fines content. In those tests a constant ratio of ρ_d/ρ_{Pr} (with the conventional dry density ρ_d and the proctor dry density ρ_{Pr}) was the basis for the comparison.

On the other hand, the prediction of the behaviour of sand-silt mixtures under critical state soil mechanics presents still challenges, because the critical state as well as the steady state is dependent on fines content (f_c). One possible reason for this is the usage of the global void ratio as a state variable. Therefore, Thevanayagam et al. [25] proposed the equivalent void ratio e^* as a more appropriate state variable, which will be further evaluated in this study.

The objective is to present a systematic experimental study on the mechanical behaviour of Karlsruhe fine sand

✉ Merita Tafili
  merita.tafili@rub.de

1   Chair of Soil Mechanics, Foundation Engineering and Environmental Geotechnics Ruhr-University Bochum, Bochum, Germany

2   Keller Grundbau GmbH, Renchen, Germany

3   Institute of Soil Mechanics and Rock Mechanics, Karlsruhe Institute of Technology, Karlsruhe, Germany

mixed with 10% and 20% low-plastic Kaolinite with a plasticity index $I_P = 12.2\%$ calculated as the difference between the liquid limit and the plastic limit. Drained and undrained monotonic triaxial tests, as well as drained high-cyclic tests are presented and analyzed. For comparison purposes some experimental results of the pure materials Karlsruhe fine sand as well as Kaolinite are used. Thereby, the influence of low-plastic Kaolinite on the behaviour of Karlsruhe fine sand is evaluated using the phase transformation angle, the critical void ratio, the secant Young's modulus, the residual strain accumulation as well as strain amplitude during drained cycles. Different void ratio approaches are compared, whereby the equivalent void ratio proposed by Thevanayagam et al. [25] is found to be more appropriate as a state variable. Some oedometric tests on the same materials are published in Tafili et al. [23]. The presented data and experimental results can be used for the development of new constitutive models for sand-silt mixtures either conventional or high cyclic accumulation models, or for the calibration and validation of existing models.

2 Void ratios

The global void ratio, defined as the ratio between the pore volume to the volume of solids:

$$e = \frac{V_P}{V_S} \tag{1}$$

is used in soil mechanics as a density parameter to characterize soil behavior. However, it has been demonstrated [3, 5, 8, 16, 24, 34] that this approach is insufficient for the behavior of mixtures including coarse and fine-grained soils. One reason is that fine grains are considered part of the soil skeleton in Eq. (1). The fine grains, on the other hand, accumulate in the pores and settle between the coarse grains only when the fines content increases. To account for this, various methods for the calculation of the void ratio of sand-silt mixtures were developed.

2.1 Skeleton void ratio

The skeleton void ratio (used in literature as e_g [8, 24] or as e_{skeleton} [5]) is defined under the assumption that the fines are located in voids formed by sand grains [34]. As a result, the fine grains are assumed to be inactive and to act as voids. Different methods of calculation were presented in Kuerbis [8], Hight et al. [5], Thevanayagam [24]:

$$e_g = \frac{e + f_c}{1 - f_c} \tag{2}$$

$$e_{\text{skeleton}} = \frac{V_T G_S \rho_W - (M - M_f)}{(M - M_f)} \tag{3}$$

$$e_g = \frac{V_P + V_{f_c}}{V_S} \tag{4}$$

with the fines content f_c, total volume of the sample V_T, specific gravity of the soil G_S, density of water ρ_w, total soil mass M, fines mass M_f and volume of fines V_{f_c}. It has been shown [3] that the various formulars for the skeleton void ratio do not differ fundamentally.

2.2 Equivalent void ratio

The assumption of inactive fine grains can only be justified if a small amount of fines content is present. With an increasing content of fines, the finer fraction of grains will start to settle between the coarse grains and will be actively involved in the load transfer. To account for this, the equivalent void ratio proposed by Thevanayagam et al. [25] is widely used:

$$e^* = \frac{e + (1-b)f_c}{1 - (1-b)f_c} \tag{5}$$

where b represents the fraction of fines that are active in force structure. It depends on the grain size distribution curve and the threshold fines content f_{thre} [16]:

$$b = \left[1 - \exp\left(-0.3 \cdot \frac{(f_c/f_{\text{thre}})}{k}\right)\right] \cdot \left(r \cdot \frac{f_c}{f_{\text{thre}}}\right)^r \tag{6}$$

with

$$\chi = \frac{D_{10}}{d_{50}}, \qquad r = \frac{1}{\chi} \qquad \text{and} \qquad k = 1 - r^{0.25} \tag{7}$$

The particle size ratio χ describes the mixture of coarse and fine grains, while D_{10} is taken out of the grain size distribution of the coarse grain material and d_{50} of the fine grain material. Equation (5) reduces to the skeleton void ratio in Eq. (2) for $b = 0$.

The threshold fines content f_{thre} describes the transition of the soil behavior from a coarse grained material with fines to a fine grained material with coarse grains. If the threshold fines content is exceeded, the coarse grains will no longer participate in the load transfer, but float between the fine grains. Therefore the concept of the equivalent void ratio is only applicable if the fines content f_c remains under the threshold fines content [18].

Mathematically, f_{thre} is formulated by means of the steady state line (SSL). It was observed that the slope of SSL of a soil changes depending on the fines content. In the study presented in Rahman and Lo [16], Rahman et al. [17], the SSL first moves downwards with increasing fines content. Above a certain content of fines, the SSL becomes

steeper again. The fines content, at which the SSL slope reaches its minimum, is referred to as the threshold fines content *thre*:

$$f_{\text{thre}} = 0.40\left(\frac{1}{1 + e^{\alpha - \beta\chi}} + \frac{1}{\chi}\right) \qquad (8)$$

The parameters α and β were determined by Rahman et al. [15] using several laboratory data from literature to $\alpha = 0.50$ and $\beta = 0.13$. As an initial approximation, f_{thre} can be assumed in the range of 30–41% [12, 13, 16].

3 Materials, sample preparation and testing devices

The tested materials consist of Karlsruhe fine sand (abbreviated as KFS) mixed with different quantities of Kaolinite (abbreviated as K) to achieve a fines content of 10% and 20%. The grain size distribution curves of all materials are presented in Fig. 1. Assuming $\alpha = 0.50$ and $\beta = 0.13$ and considering the grain size distribution curves in Fig. 1 ($\chi = 26.5$), the threshold fines content is determined to $f_{\text{thre}} = 39.5\%$. The same fine sand has been used for the extensive experimental data base presented in Wichtmann and Triantafyllidis [28], Wichtmann and Triantafyllidis [29], while the Kaolinite employed herein has also been used as a pure silt material (hence low to non-plastic fines) in the detailed experimental study conducted in Wichtmann and Triantafyllidis [30].

The tests in the following sections were carried out on samples with a diameter of 10 cm and a height of 10 cm in two distinct triaxial testing devices. In Fig. 2a, a system for monotonic loading is illustrated, and in Fig. 2b, a scheme for cyclic loading is shown. The difference between the devices lies in the method of load application. The axial force is applied from above via a spindle gear in the monotonic device. The cyclic load mechanism, on the other hand, is controlled by a pneumatic cylinder placed beneath the cell. The vertical load is measured at a load cell outside (Fig. 2a) respectively located directly below the sample base plate (Fig. 2b). Vertical displacement is measured with a displacement transducer with an accuracy and resolution of 10 μm mounted to the load piston. System deformation has been carefully determined in preliminary tests on a steel dummy and subtracted from the measured displacements. The samples were tested fully water-saturated and volume changes were obtained from the squeezed out or sucked in pore water using a system of two burettes (one connected to the drainage lines, one with constant water level) and a differential pressure transducer. The end plates were equipped with small central porous stones (diameter 15 mm). The friction at the end plates was reduced by smearing the end plates with a thin layer of grease followed by a latex rubber disk of 0.4 mm thickness similar to Wichtmann [27] for reducing failure at the end plates. Latex membranes of 0.4 mm thickness were used to surround the sample. The application of the stress paths can lead to membrane penetration effects [10, 26]. These were
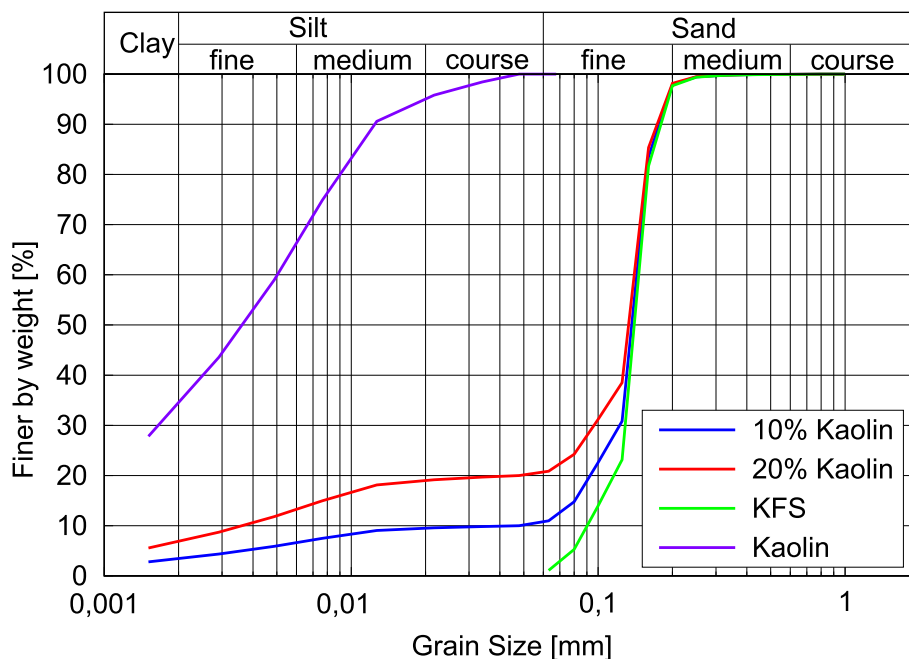
Fig. 1 Grain size distribution curves of Karlsruher Finesand (KFS), Kaolinite, Karlsruher Finesand with 10% Kaolinite and Karlsruher Finesand with 20% Kaolinite

a)

b)
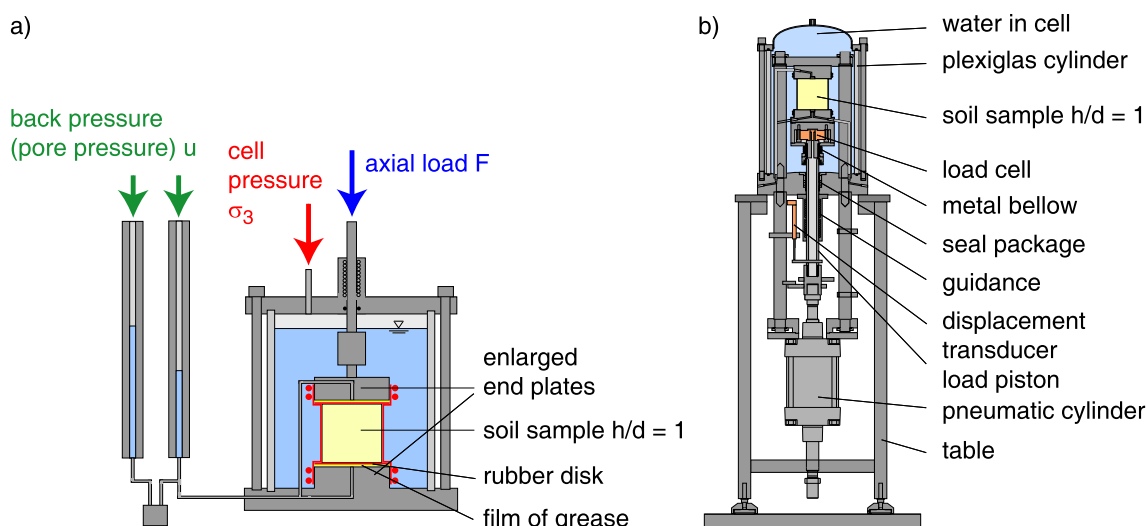
Fig. 2 Scheme of triaxial testing devices for **a** monotonic and **b** cyclic loading at IBF, KIT

Table 1 Program of triaxial tests

Material	Monotonic undrained	e_0^*	Monotonic drained	e_0^*	High-cyclic drained	e_0^*
KFS + 10% Kaolinite	M16	0.848	M23	0.874	C01	0.942
	M06	0.952	M02	0.975	C03	0.952
	M15	0.969	M04	1.073	C02	1.066
	M21	0.921	M01	0.932		
	M22	0.957	M07	0.989		
	M05	1.081	M03	1.074		
KFS + 20% Kaolinite	M18	0.875	M10	0.933	C07	0.906
	M13	0.939	M20	0.976	C05	1.074
	M19	1.045	M08	1.055	C011	1.091
	M17	0.895	M11	0.934		
	M12	1.043	M09	1.050		
	M14	1.072				

Equivalent void ratios e_0^* measured at initial mean pressure $p_0' = 100$ kPa prior to shearing

found to be negligible for $d_{50} = 0.14$ mm [11]. The samples were prepared by moist tamping in eight layers with a 10% degree of undercompaction and tested in a water-saturated state with a back pressure of $u = 500$ kPa.

Before the separate layers could be tamped down, KFS blends containing 10 or 20% Kaolinite were created. Both materials were mixed in a stirrer (Kitchen Aid) with the addition of distilled and demineralized water. Despite open drainage, the blends with 30% Kaolinite showed excessive pore water pressures in monotonic testing with the loading rate $v = 0.1$ mm/min and in cyclic testing with a loading frequency $f = 0.2$ Hz, therefore they were not examined in this research.

In both types of triaxial tests, the effective lateral stress $\sigma_2 = \sigma_3$ was kept constant, while the monotonic and the cyclic loading was applied in the vertical direction as σ_1. For cyclic tests, an average value of effective axial stress

$\sigma_1'^{av}$ and a stress amplitude $\sigma_1'^{ampl}$ was applied. In the following the stress conditions in the drained cyclic tests are described by the average mean pressure p'^{av} (with $p' = (\sigma_1 + 2\sigma_3)/3$), the average deviatoric stress q^{av} (with $q = \sigma_1 - \sigma_3$), average stress ratio $\eta^{av} = q^{av}/p^{av}$ and deviatoric stress amplitude $q^{ampl} = \sigma_1^{ampl}$.

4 Tests with montonic loading

In the following, undrained as well as drained monotonic triaxial tests with monotonic loading are presented. The testing programme comprise 12 undrained and 11 drained monotonic triaxial tests with variation of fines content between 10 and 20% as well as initial void ratio as listed in Table 1.
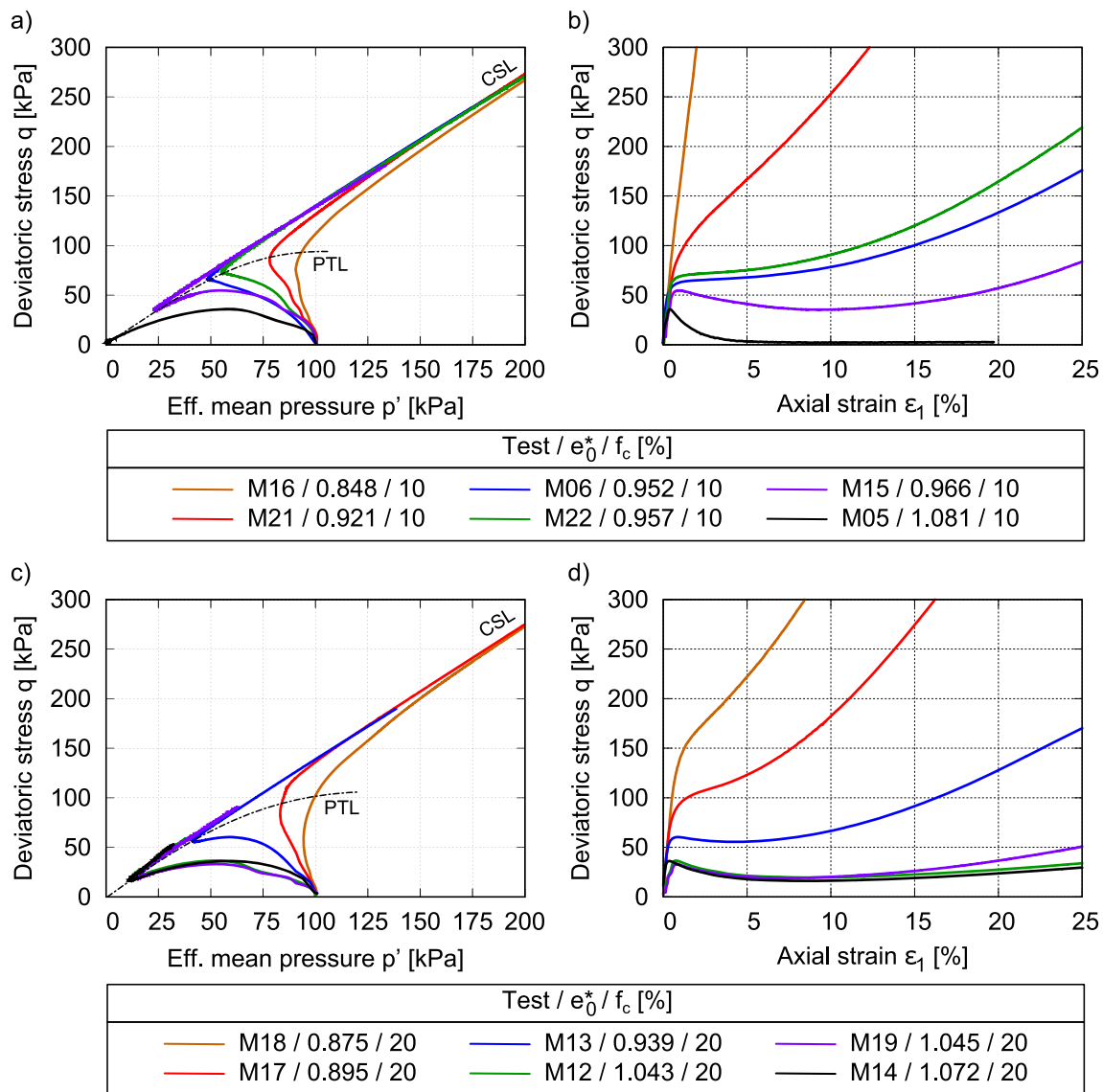
Fig. 3 Deviatoric stress q over eff. mean pressure p' or axial strain ε_1 in undrained monotonic triaxial tests starting from an initial mean pressure $p'_0 = 100$ kPa on **a**, **b** KFS with 10% K and **c**, **d** KFS with 20% K

4.1 Undrained triaxial tests

All samples were prepared by moist tamping, as described previously. For the following undrained triaxial tests they were isotropically consolidated at $p'_0 = 100$ kPa and sheared with a displacement rate of 0.1 mm/min. The initial equivalent void ratio was varied between $e^* = 0.875$ and 1.081.

The measured curves of deviatoric stress q versus effective mean pressure p' as well as versus the axial strain ε_1 are presented in Fig. 3. Both mixtures show, as expected, an increasing dilatancy and shear strength with increasing initial density, hence decreasing void ratio. A comparison with the undrained effective stress paths in Wichtmann and Triantafyllidis [28], Wichtmann and

Triantafyllidis [29], Wichtmann and Triantafyllidis [30] for pure KFS or pure K reveal that the paths in Fig. 3 are similar to those of KFS rather than K. The very loose sample of KFS + 10% K (test M05) shows a purely contractive behaviour leading to a full liquefaction (i.e. $p' = q = 0$ kPa), as observed for sand samples prepared by moist tamping [6, 22, 27]. On the other side, the loosest samples of KFS + 20% K (tests M12, M14 and M19) reach low effective stresses but not a full liquefaction, as expected rather for fine-grained soils. Hence, with increasing fines content the influence of the fines on the mechanical behaviour of the mixture is more pronounced.

In case of the samples with lower equivalent void ratios (tests M16, M21 and M17, M18) the slight contractive tendency observed during the initial stage of the tests is
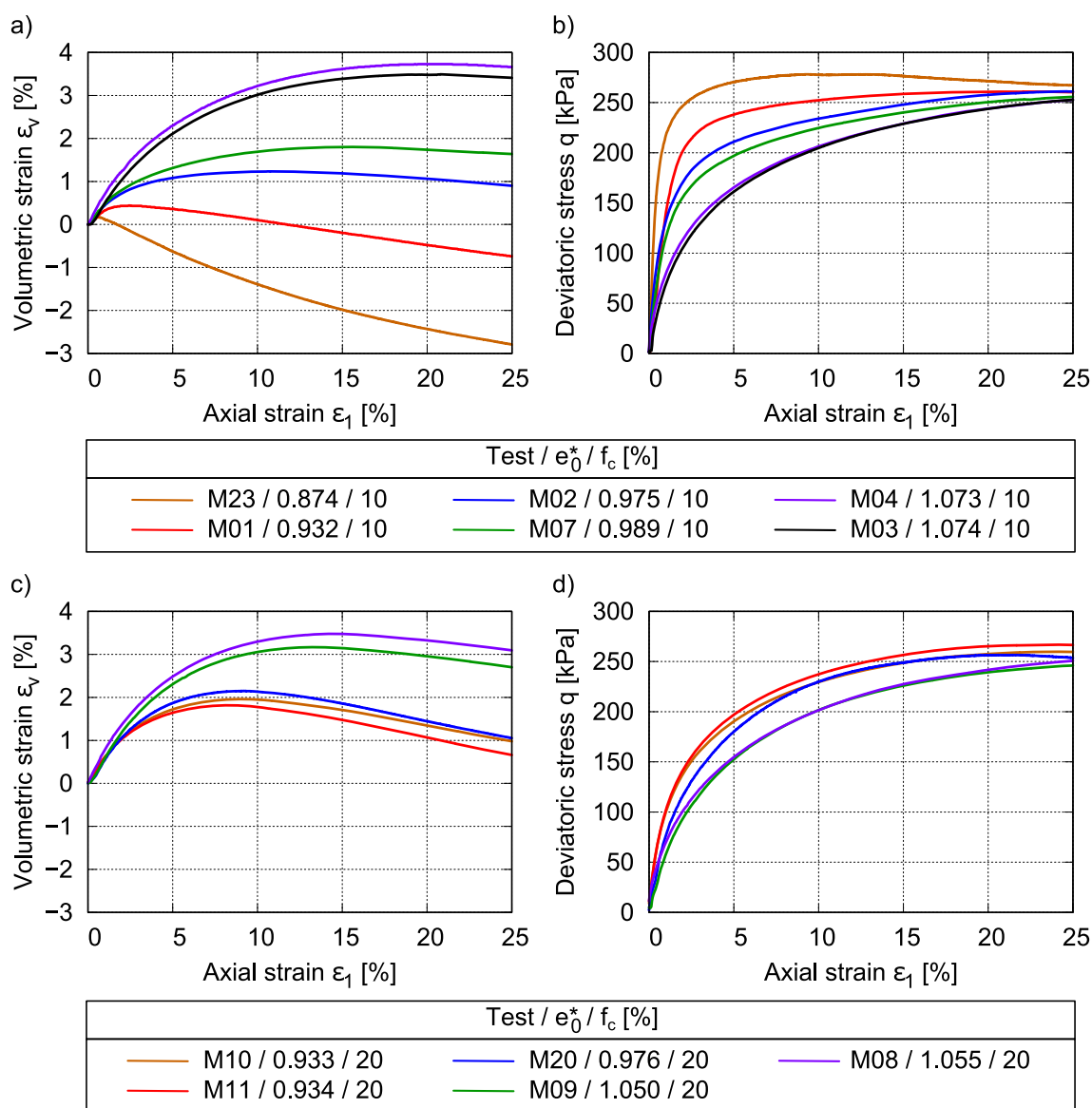
Fig. 4 Volumetric strain ε_v or deviatoric stress q over axial strain ε_1 in drained monotonic triaxial tests starting from an initial mean pressure $p'_0 = 100$ kPa on **a**, **b** KFS with 10% K and **c**, **d** KFS with 20% K

followed by dilatancy at larger strains. For intermediate void ratios (tests M06, M15, M22 and M13) the behaviour is purely contractive at larger pressures while predominantly dilative at lower p' values.

A comparison of Fig. 3b, d reveals that for a given equivalent void ratio, the initial slope of the q-ε_1 relationship for the mixtures containing 10% K is steeper than that of the mixtures with 20% K, which is in agreement with other studies [3, 8]. Irrespectively of the void ratio, the final effective stress states at large strains ($\varepsilon_1 \geq 25\%$) are similar, which is in agreement with the critical state. The data shown in Fig. 3 look similar to those of Yang et al. [34], Rahman et al. [15] which are frequently used for the development as well as calibration of constitutive models

in the literature. However, most of the initial pressures used in the present test series are lower than those applied in Yang et al. [34], Rahman et al. [15] ($p'_0 = 350, 500, 1150$ kPa). The p'_0-range combined with the variation of e^*_0, which are examined in the present test series, are thought to be of higher practical relevance for most in situ problems. Furthermore, this study includes laboratory tests with different load controls and drainage conditions.

4.2 Drained triaxial tests

In the following, the results of 11 drained monotonic triaxial tests with variation of initial equivalent void ratio in the range of $0.874 \leq e^* \leq 1.074$ are presented. The samples
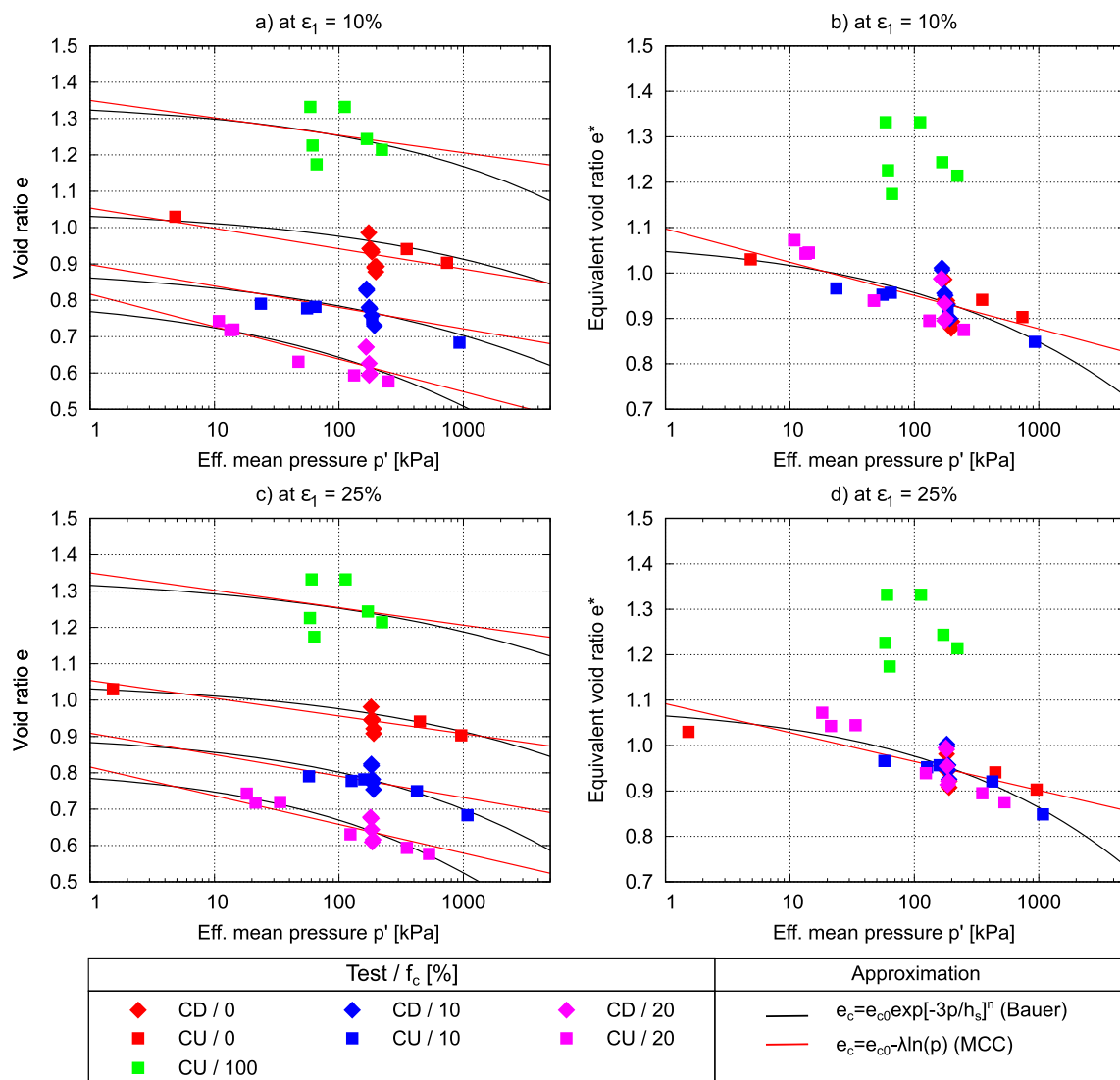
Fig. 5 Eff. mean pressure p' versus **a** void ratio e and **b** equivalent void ratio e^* at axial strain $\varepsilon_1 = 10\%$ and **c** and **d** at axial strain $\varepsilon_1 = 25\%$ in monotonic triaxial tests on KFS with 0, 10 and 20%. Approximation with Eqs. (9) and (10) as well as parameters from Table 2

of KFS with different amounts of K (10%, 20%) were prepared by moist tamping and were sheared from an initial mean effective pressure of $p'_0 = 100$ kPa.

Figure 4 presents the measured curves of both volumetric strain ε_v and deviatoric stress q versus the axial strain ε_1. The well known tendency of increasing volumetric strain ε_v, hence decreasing dilatancy with decreasing initial relative density [32, 36] is well reproduced by these laboratory tests. Furthermore, the samples with 20% fines content show a higher volumetric strain ε_v compared to mixtures with 10% fines content at a similar initial equivalent void ratio e^*. The $q - \varepsilon_1$ paths in Fig. 4b and d reveal an increasing initial stiffness and shear strength with decreasing fines content. Nevertheless, the shear strength in the residual state is identical for both mixtures, which may

be considered as an indication of the presence of similar critical state parameters.

4.3 Evaluation of the impact of void ratio definition on the critical void ratio

In the following, all tests presented in Figs. 3 and 4 (mixtures), as well as laboratory data from Wichtmann and Triantafyllidis [28], Wichtmann and Triantafyllidis [29], Wichtmann and Triantafyllidis [30] (pure KFS–red color or Kaolinite– green color) are used for the evaluation of the void ratio at different strain levels $\varepsilon_1 = 10$ and 25%. These values of the axial strain were considered in order to examine the influence of the fines content on the critical void ratio, which, however, might vary due to inhomogeneous strain distribution within the sample at higher strains.

Table 2 Parameters of the fitted Eqs. (9) and (10) for Fig. 5

Material	ε_1 [%]	e_{c0}	e_{c0}^*	h_s [MPa]	n	λ
KFS + 0% Kaolinite	10	1.054	–	4000	0.27	0.024
	25	1.054	–	4000	0.27	0.021
KFS + 10% Kaolinite	10	0.898	–	726	0.26	0.026
	25	0.909	–	197	0.32	0.026
KFS + 20% Kaolinite	10	0.817	–	37	0.30	0.039
	25	0.816	–	31	0.35	0.034
100% Kaolinite	10	1.350	–	2594	0.29	0.021
	25	1.350	–	21111	0.23	0.021
KFS + 0%/10%/20% Kaolinite	10	–	1.079	328	0.30	0.032
	25	–	1.092	260	0.32	0.028

The abbreviations CU and CD stand for undrained and drained monotonic triaxial test, respectively.

Figure 5 presents the void ratio e (on the left column) and the equivalent void ratio e^* (on the right column) versus the effective mean stress p' of all monotonic triaxial tests at the critical state for different amounts of fines content (0, 10, 20 and 100%). Two approximations as possible representatives of the critical state are applied: first, the void ratios were plotted at an axial strain of $\varepsilon_1 = 10\%$ (Fig. 5a, b) and, second, of $\varepsilon_1 = 25\%$ (Fig. 5c, d). Except for the non-guaranteed homogeneity of the samples at 25% axial strain, there is no change in the trend of the $e - p'$ paths in Fig. 5.

Figure 5a, c show different critical void ratio– effective mean pressure lines for samples with different amounts of fines. The well known trend of decreasing void ratio with increasing mean effective pressure is well reproduced by these evaluations. Using the equivalent void ratio instead, the data points for 0, 10 and 20% fines content can be described by the same curve, as shown in Fig. 5b, d. Obviously, the equivalent void ratio e^* for the pure materials (KFS or K corresponding to 0 or 100% fines content, respectively) is equal to the global void ratio e. In Fig. 5, the approximation function for the critical void ratio line is approximated with both, the exponential compression law according to Bauer [1], which is usually used for sands:

$$e_c = e_{c0} \exp\left[-\left(\frac{3p}{h_s}\right)^n\right] \qquad (9)$$

and the Modified Cam Clay (MCC) type compression law, used usually for fine-grained soils

$$e_c = e_{c0} - \lambda \cdot \ln(p). \qquad (10)$$

Herein e_{c0} denotes the value of e_c for $p = 1$kPa. The granular hardness h_s, has the dimension of stress, n is a

constant and λ is the well-known compression index. The calibrated parameters are listed in Table 2.

The critical void ratio line for Kaolinite cannot be unambiguously derived using these data, since they only cover a small stress range of effective mean stress lying between $p' = 60 - 130$ kPa. Furthermore, it is not clear whether the critical state has been reached by the Kaolinite samples. The softening shown at the last stages of the effective stress paths in Wichtmann and Triantafyllidis [30] indicate inhomogeneity of the specimens.

The critical void ratio line of the sand-silt mixtures as well as pure KFS is described well by both, Bauer compression law and MCC relation. Figure 5c, d indicate a unique critical void ratio line for all tested sand-silt mixtures and KFS using the equivalent void ratio instead of the global one. This results are in good agreement with other experimental studies presented for e.g. in Rahman et al. [17].

4.4 Evaluation of the impact of void ratio definition on the phase transformation line (PTL)

This section contains the evaluation of the phase transformation line. The phase transformation angle φ_{PTL} is determined at maximum volumetric strain ε_v i.e. $- \max\left(\arctan(\dot{\varepsilon}_v/\dot{\gamma})\right)$ in drained tests, while in the undrained tests it has been evaluated at the minimum effective mean pressure p'.

In Fig. 6a, c and e φ_{PTL} is plotted versus the initial void ratio e_0, the void ratio e and the normalized void ratio with respect to the critical void ratio e/e_c, respectively, whereas in the right column of Fig. 6 φ_{PTL} is plotted versus the corresponding equivalent void ratio values. For each test the critical void ratio was determined using Eq. (9) with the parameters e_{c0}, n and h_s given in Table 2. Of course, the equivalent void ratio of pure KFS or pure Kaolinite is equal to the global void ratio. The data reveal an increasing φ_{PTL} with increasing void ratio, hence decreasing density. This is in good agreement with the literature [2, 9, 14, 21, 28].

In Fig. 6a and c, four different curves can be fitted for the four different soils. Using the equivalent void ratios in Fig. 6 b and d the pure KFS and the KFS+10% as well as KFS+20% may be described using a unique relation

$$\varphi_{PTL} = C \cdot \exp\left(a \cdot x\right) \qquad (11)$$

with the parameters C and a given in Table 3. For pure Kaolinite another curve is required, denoted in Fig. 6a and c[1]. The normalization of either the void ratio or the

---

[1] Note that for Kaolinite no equivalent void ratio has been calculated, hence the Fig. 6a, c and e coincide with Fig. 6b, d and f for this soil. Therefore, the approximation curve for this soil has been illustrated only in Fig. 6a, c and e.
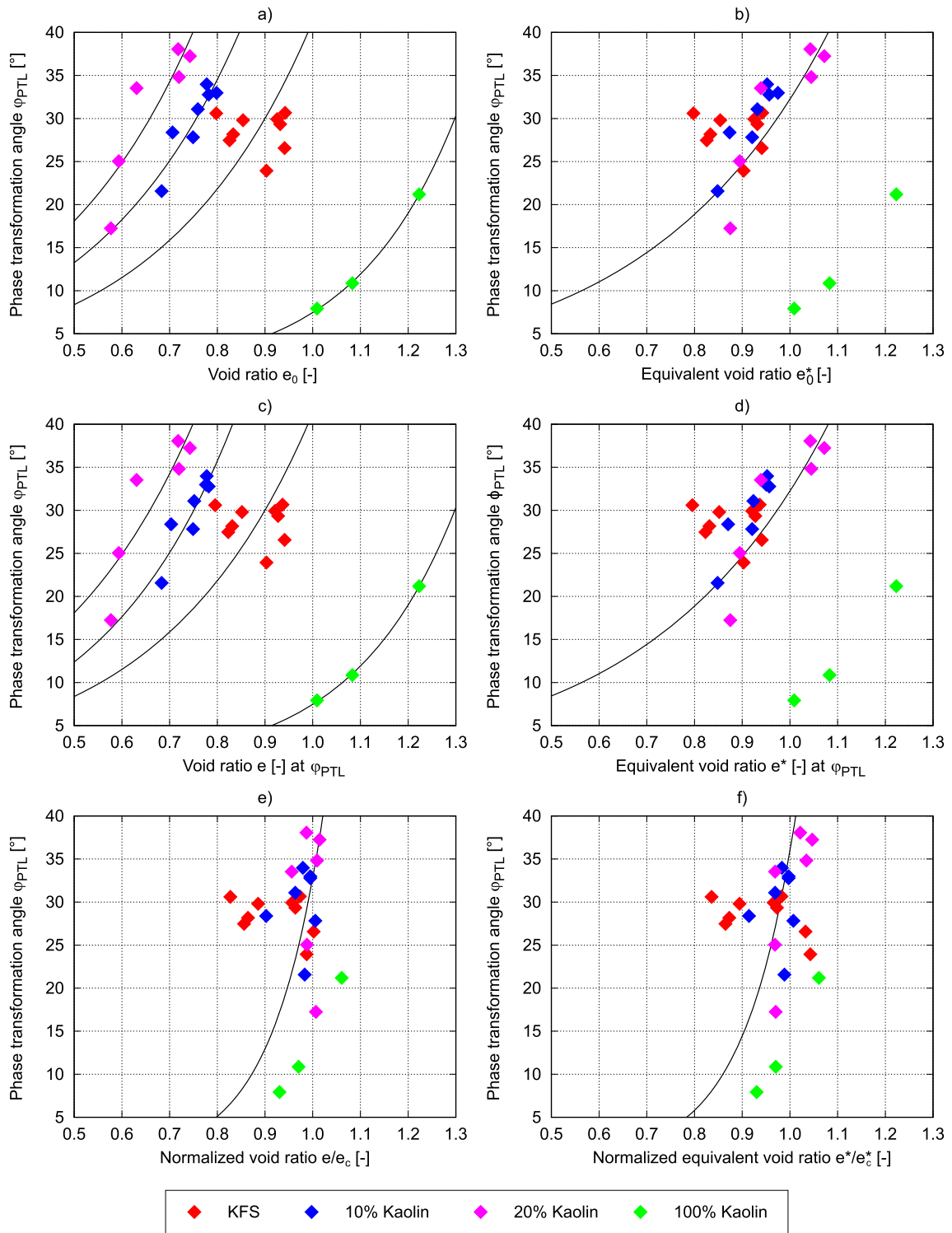
Fig. 6 φ_{PTL} versus **a** void ratio e_0, **b** equivalent void ratio e_0^*, **c** void ratio e, **d** equivalent void ratio e^*, **e** e/e_c, **f** e^*/e_c^* in drained and undrained monotonic triaxial tests on Karlsruher Finesand with 0, 10, 20 and 100% Kaolinite. Approximation with parameters after Table 3

equivalent void ratio with the critical void ratio, indicates that a unique approximation of φ_{PTL} can be found for all four soils. This is supported by the evaluations in Tafili et al. [22] based on the experimental evidence of

Wichtmann and Triantafyllidis [30], whereby the authors show that the phase transformation line of sands and clays is based on the same mechanisms and the same dilatancy

Table 3 Parameters of the fitted Eq. (11) for Fig. 6

Material	x	a	C
KFS	e_0	3.19	1.70
	e	3.19	1.70
KFS + 10% Kaolinite	e_0	3.19	2.69
	e	3.53	2.12
KFS + 20% Kaolinite	e_0	3.19	3.67
	e	3.19	3.67
100% Kaolinite	e_0	4.67	0.07
	e	4.67	0.07
KFS + 0%/10%/20% Kaolinite	e_0^*	2.68	2.21
	e^*	2.68	2.21
	e/e_c	9.30	0.003
	e^*/e_c^*	9.10	0.004

Table 4 Parameters of the fitted Eq. (13) for Fig. 7

Material	C	a
KFS + 0% Kaolinite	3400	− 5.15
KFS + 10% Kaolinite	1300	− 5.58
KFS + 20% Kaolinite	39,500	− 12.65
100% Kaolinite	13,500	− 5.92
KFS + 0%/10%/20% Kaolinite	3000	− 5.19

$$E_{50} = \frac{q_{50}}{\varepsilon_{1,50}} \tag{12}$$

The system compliance has been determined in preliminary tests on a steel dummy and considered in the evaluation of E_{50}. The data in Fig. 7 reflect the well-known increase of the initial stiffness with increasing density, i.e. decreasing void ratio.

While in Fig. 7 a four different approximation curves

$$E_{50} = C \cdot \exp(a \cdot e_0) \tag{13}$$

with the constants C and a can be fitted depending on the fines content, a unique function may be found in Fig. 7b using the initial equivalent void ratio e_0^* instead of e_0. The calibrated constants are listed in Table 4. Furthermore, Fig. 7b reveals that with decreasing initial equivalent void ratio the secant Young's modulus increases, independently of the fines content of the sample. This is important for the development of constitutive models for sand-silt mixtures, because the equivalent void ratio can be used instead of the global void ratio.

rule (with different parameters) can be adopted in constitutive models.

While the choice of void ratio definition is important for the critical void ratio, both approaches can be used as state variables for the phase transformation line.

4.5 Evaluation on the impact of void ratio definition on the secant Young's modulus E_{50}

As a measure of the initial stiffness, Young's modulus E_{50} for undrained as well as drained monotonic tests of the four considered soil types is presented as a function of void ratio e_0 or equivalent void ratio e_0^* in Fig. 7a and b, respectively. E_{50} represents a secant stiffness between $q = 0$ and $q = q_{\max}/2$ (before softening for undrained tests) [29]:

Fig. 7 **a** E_{50} versus void ratio e_0, **b** E_{50} versus equivalent void ratio e_0^* in drained and undrained monotonic triaxial tests on Karlsruher Finesand with 0, 10, 20 and 100% Kaolinite
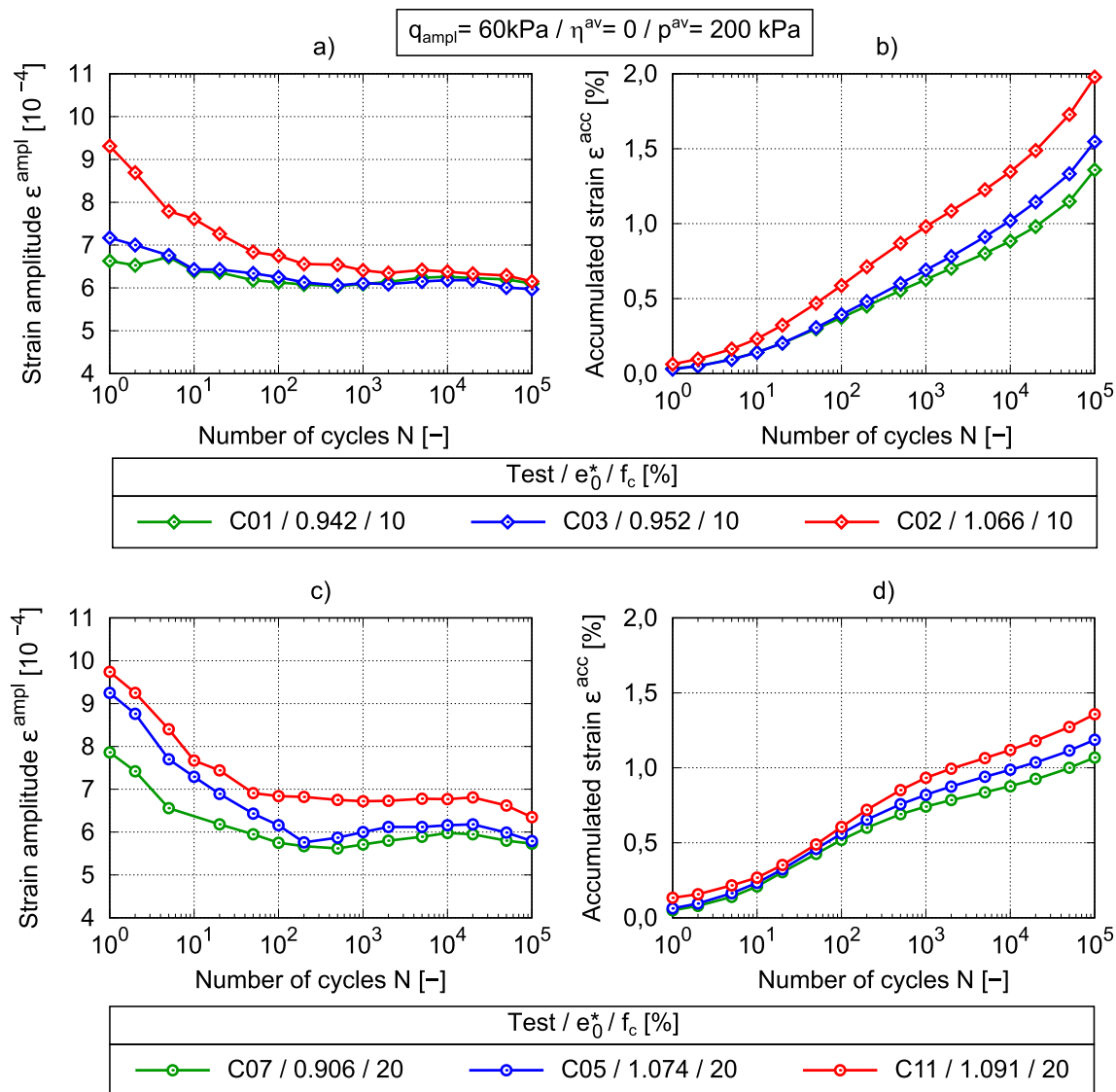
Fig. 8 Drained high-cyclic triaxial tests on KFS-K mixtures: **a** Strain amplitude $\varepsilon^{\mathrm{ampl}}$ versus number of cycles N for $f_c = 10\%$ and **c** 20%, **b** Accumulated strain $\varepsilon^{\mathrm{acc}}$ versus number of cycles N for $f_c = 10\%$ and **d** 20%

5 Tests with cyclic loading

As a continuation of the work on the influence of fines content on the behaviour of KFS, the influence of K on the cumulative deformations has been investigated with 6 high-cyclic triaxial tests considering $N = 10^5$ drained cycles on KFS+10% and 20% K.

5.1 Drained triaxial tests with high-cyclic loading

A program of the high-cyclic triaxial tests with $N = 10^5$ drained cycles, deviatoric stress amplitude of $q^{\mathrm{ampl}} = 60$ kPa, effective stress ratio of $\eta^{\mathrm{av}} = 0$ and $p'^{\mathrm{av}} = 200$ kPa is presented in Table 1. Both mixtures have been tested with various initial densities.

The diagrams in Fig. 8a, b present the results of tests performed on KFS+10% K and in Fig. 8c, d results of tests performed on KFS+20% K. While the strain amplitude $\varepsilon^{\mathrm{ampl}}$ shows a considerable increase at the first cycle with increasing initial equivalent void ratio, the difference is hardly noticeable at $N = 10^5$ cycles for different e_0^*. The mixtures with $f_c = 20\%$ reach slightly larger strain amplitudes than the mixtures with $f_c = 10\%$. Furthermore, after nearly 200 cycles $\varepsilon^{\mathrm{ampl}}$ of each mixture reachs a constant value merely independently of initial density.

The accumulated strain $\varepsilon^{\mathrm{acc}}$ documented in Fig. 8b,d increases with an increasing number of cycles, however the samples with 20% Kaolinite indicate an overall lower accumulated axial strain at 10^5 cycles than the samples with 10% Kaolinite at a similar initial equivalent void ratio.
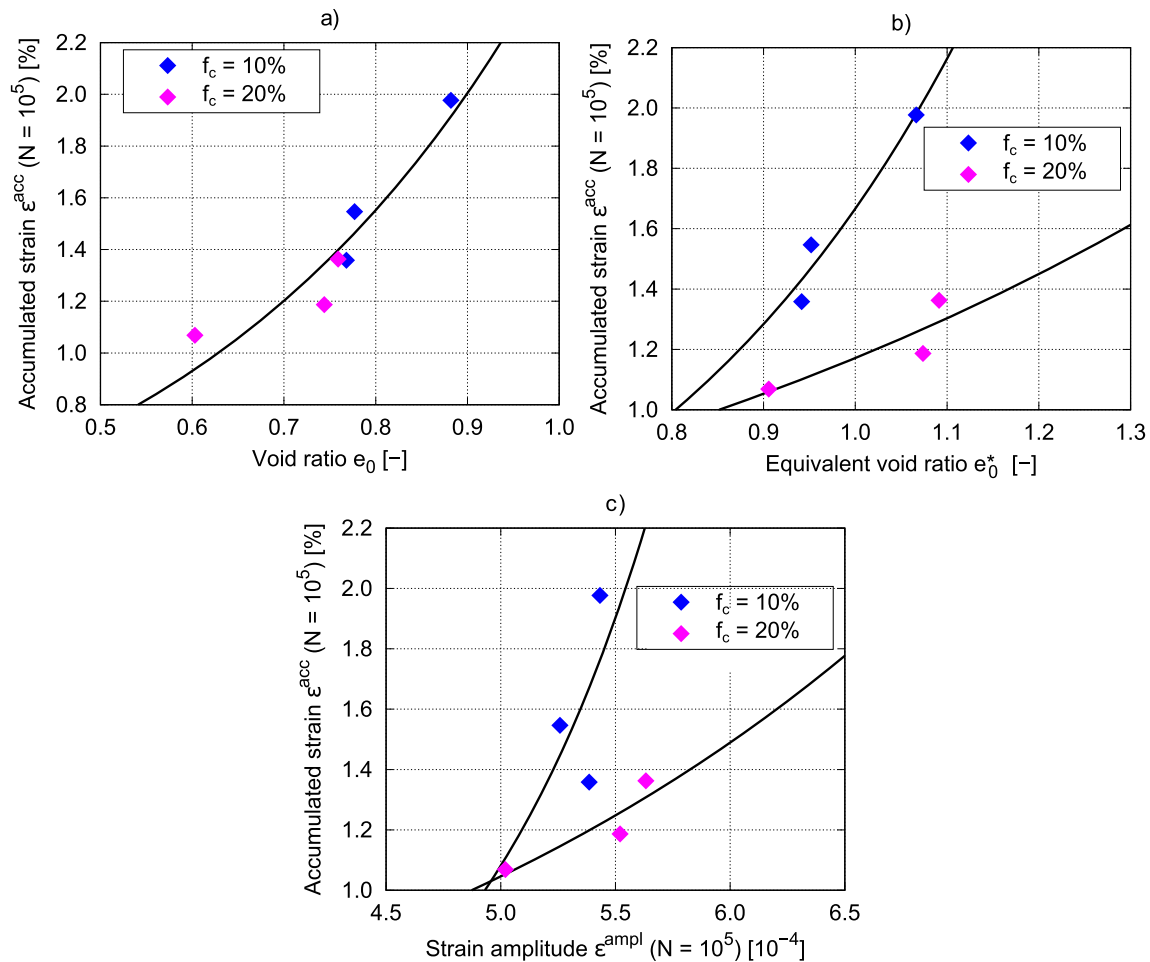
Fig. 9 Accumulated strain ε^{acc} at $N = 10^5$ cycles versus **a** void ratio e_0 **b** equivalent void ratio e_0^* and **c** strain amplitude ε^{ampl} at $N = 10^5$ cycles for the tests presented in Fig. 8

Table 5 Parameters for Fig. 9 a, Eq. (14), Fig. 9 b, Eq. (15) and for Fig. 9 c, Eq. (16)

Material	Fig. 9a		Fig. 9b		Fig. 9c	
	C	a	C	a	C	a
Karlsruher Finesand + 10% Kaolinite	2.000	2.559	0.123	2.608	0.004	1.130
Karlsruher Finesand + 20% Kaolinite			0.404	1.066	0.179	0.353

The residual strains measured for the various initial test conditions after $N = 10^5$ cycles are compared in Fig. 9. These diagrams confirm the increase of ε^{acc} with growing initial void ratio. In Fig. 9b two relations between the accumulated strain ε^{acc} and the initial equivalent void ratio e_0^* depending on fines content have been established, see Tab. 5. These results reveal an increasing ε^{acc} with increasing f_c when evaluated regarding e_0^*. While, Fig. 9a shows an increasing ε^{acc} with e_0 independently on f_c.

Hence, unlike in the previously described experiments, a unique relationship between ε^{acc} and the initial global void ratio e_0 can be identified. The parameters for the equations

$$\varepsilon^{acc} = C \cdot \exp(a \cdot e_0) \tag{14}$$

$$\varepsilon^{acc} = C \cdot \exp(a \cdot e_0^*) \tag{15}$$

$$\varepsilon^{acc} = C \cdot \exp(a \cdot \varepsilon^{ampl}) \tag{16}$$

are listed in Table 5. Figure 9c shows increasing strain amplitudes with increasing residual strain accumulation and was approximated with two parameter sets for each f_c, see Table 5.

6 Concluding remarks

This paper presents both undrained and drained triaxial tests with monotonic as well as high cyclic loading of sand-silt mixtures with 10 and 20% fines content. The materials used for the experiments consist on Karlsruhe fine sand

(tested in detail in Wichtmann and Triantafyllidis [28], Wichtmann and Triantafyllidis [29]) and Kaolinite (experimental database available from Wichtmann and Triantafyllidis [30]).

The undrained triaxial laboratory tests indicate that the considered mixtures behave under mechanical loading like the coarser fraction, the Karlsruhe fine sand. Furthermore, for loose samples a full liquefaction state has been reached, contrary to the behavior of pure Kaolinite. In addition, the dilatancy in drained triaxial shearing decreases with increasing fines content for the same initial equivalent void ratio. Using the initial equivalent void ratio a unique critical void ratio relation as well as phase transformation line could be established for all considered materials. The evaluation of Young's modulus revealed its increase with decreasing equivalent void ratio without distinguishing between different fines contents. Hence, a unique relation between E_{50} and the equivalent void ratio was indicated as well, which can be used for the development of constitutive models.

Six drained tests with each 10^5 cycles revealed, besides the well known dependencies, an increase of the residual strain accumulation with decreasing fines content at the same initial equivalent void ratio. However, a unique and on f_c independent relationship between ε^{acc} could be found only with respect to the initial global void ratio e_0. This is surprising compared to the results from monotonic tests and implies that for lower strains (here tested up to 2.2 % accumulated strain), the fines content plays a significant role in the load transfer since the finer grains may settle in the contact zone between the coarse grains. While, for loading involving higher plastic deformations (monotonic loading) the mechanical properties are less influenced by the fine grains which due to the higher loading and deformation level are displaced from the contact zone.

Since the equivalent initial void ratio has proven to provide a suitable state variable for the evaluation of the mechanical behavior of the considered sand-silt mixtures under monotonic loading, the development, modification or validation of implicit constitutive models using this experimental database is now of great interest. On the other side, the validation or development of explicit high-cycle models requires further investigations.

Data availibility Some or all data that support the findings of this study are available from the corresponding author upon reasonable request.

References

1. Bauer E (1996) Calibration of a comprehensive hypoplastic model for granular materials. Soils Found 36(1):13–26
2. Been K, Jefferies M (1985) A state parameter for sands. Géotechnique. 35(2):99–112
3. Chu J, Leong WK (2002) Effect of fines on instability behaviour of loose sand. Géotechnique 52(10):751–755
4. Coop M, Atkinson J, Taylor R (1995) Strength and stiffness of structured and unstructured soils. In: Proceeding of 11th European international conference soil mechanics and foundation engineering, Copenhagen, vol 1, pp 55–62
5. Hight D, Burland J, Georgiannou V (1990) The undrained behaviour of clayey sands in triaxial compression and extension. Géotechnique 40:431–449
6. Ishihara K (1993) Liquefaction and flow failure during earthquakes. The 33rd rankine lecture. Géotechnique 43:351–415
7. Ishihara K, Troncoso J (1980) Cyclic strength characteristics of tailings materials. Soils Found 20:127–142
8. Kuerbis RH (1989) The effect of gradation and fines content on the undrained loading response of sand. Ph.D. thesis, University of British Columbia, https://open.library.ubc.ca/collections/ubctheses/831/items/1.0062832
9. Li X, Dafalias Y (2000) Dilatancy for cohesionless soils. Géotechnique 50(4):449–460
10. Nicholson P, Seed R, Anwar H (1993) Elimination of membrane compliance in undrained triaxial testing. I. measurement and evaluation. Can Geotech J 30(5):727–738
11. Niemunis A, Knittel L (2020) Removal of the membrane penetration error from triaxial data. Open Geomech 2(5):1–13
12. Porcino DD, Triantafyllidis T, Wichtmann T, Tomasello G (2021) Application of critical state approach to liquefaction resistance of sand-silt mixtures under cyclic simple shear loading. J Geotech Geoenviron Eng 147(3):04020177
13. Porcino DD, Triantafyllidis T, Wichtmann T, Tomasello G (2022) Using different state parameters for characterizing undrained static and cyclic behavior of sand with non-plastic fines. Soil Dyn Earthq Eng 159:107318
14. Pradhan T, Tatsuoka F, Sato Y (1989) Experimental stress-dilatancy relations of sand subjected to cyclic loading. Soils Found 29(1):45–64
15. Rahman MM, Lo S-C, Baki M (2011) Equivalent granular state parameter and undrained behaviour of sand-fines mixtures. Acta Geotech 6:183–194

16. Rahman MM, Lo SR (2008) The prediction of equivalent granular steady state line of loose sand with fines. Geomech Geoeng 3(3):179–190

17. Rahman MM, Lo SR, Gnanendran C (2008) On equivalent granular void ratio and steady state behaviour of loose sand with fines. Can Geotech J 45(10):1439–1456

18. Rahman MM, Lo SR, Gnanendran CT (2009) Reply to the discussion by wanatowski and chu on "on equivalent granular void ratio and steady state behaviour of loose sand with fines. Can Geotech J 46(4):483–486

19. Rahmani H, Naeini S (2020) Influence of non-plastic fine on static iquefaction and undrained monotonic behavior of sandy gravel. Eng Geol 275:105729

20. Shi X, Herle I (2017) Undrained shear strength and water content distribution of remoulded clay mixtures. Geotechnik 40(1):60–63

21. Tafili M (2020) On the behaviour of cohesive soils: constitutive description and experimental observations. PhD Thesis, Heft 186, Veröffentlichungen des Instituts für Bodenmechanik und Felsmechanik am Karlsruher Institut für Technologie (KIT)

22. Tafili M, Grandas C, Triantafyllidis T, Wichtmann T (2021a) On the dilatancy of fine-grained soils. Geotechnics 1(1):192–215

23. Tafili M, Knittel L, Gauger V (2021b) Experimentelle und numerische Untersuchungen zum Kompressionsverhalten von Sand-Schluff-Gemischen. Geotechnik.(in print) https://doi.org/10.1002/gete.202100006

24. Thevanayagam S (1998) Effect of fines and confining stress on undrained shear strength of silty sands. J Geotech Geoenviron Eng 124(6):479–491

25. Thevanayagam S, Shenthan T, Mohan S, Liang J (2002) Undrained fragility of clean sands, silty sands, and sandy silts. J Geotech Geoenviron Eng 128(10):849–859

26. Tokimatsu K (1990) System compliance correction from pore pressure response in undrained cyclic triaxial tests. Soils Found 30(2):14–22

27. Wichtmann T (2016) Soil behaviour under cyclic loading-experimental observations, constitutive description and applications. Veröffentlichungen des Instituts für Bodenmechanik und Felsmechanik am KIT. Habilitation, Heft, p 181

28. Wichtmann T, Triantafyllidis T (2016a) An experimental data base for the development, calibration and verification of constitutive models for sand with focus to cyclic loading. Part I: tests with monotonic loading and stress cycles. Acta Geotech 11(4):739–761

29. Wichtmann T, Triantafyllidis T (2016b) An experimental data base for the development, calibration and verification of constitutive models for sand with focus to cyclic loading. Part II: tests with strain cycles and combined loading. Acta Geotech 11(4):763–774

30. Wichtmann T, Triantafyllidis T (2018) Monotonic and cyclic tests on kaolin: a database for the development, calibration and verification of constitutive models for cohesive soils with focus to cyclic loading. Acta Geotech 13:1103–1128

31. Xenaki V, Athanasopoulos G (2003) Liquefaction resistance of sand-silt mixtures: an experimental investigation of the effect of fines. Soil Dyn Earthq Eng 23(3):1–12

32. Xiao Y, Xiang J, Liu H, Ma Q (2017) Strength-dilatancy relation of sand containing non-plastic fines. Géotech Lett 7:204–210

33. Yamamuro J, Lade P (1998) Steady-state concepts and static liquefaction of silty sands. J Geotech Geoenviron Eng 124(9):868–877

34. Yang J, Wei L, Dai B (2015) State variables for silty sands: global void ratio or skeleton void ratio? Soils Found 55(1):99–111

35. Yee E, Duku M, Stewart J (2014) Cyclic volumetric strain hebavior of sands with fines of low plasticity. J. Geotech. Geoenviron. Eng. ASCE 140:1–10

36. Yilmaz Y, Yibing D, Chang C, Aydin H (2021) Strength-dilatancy and critical state behaviours of binary mixtures of graded sands influenced by particle size ratio and fines content. Géotechnique 16:1–16